IR Spectra of Phosphate Ions in Aqueous Solution: Predictions of a DFT/MM Approach Compared with Observations

Marco Kl̈ahn,[†] Gerald Mathias,[‡] Carsten Kötting,[†] Marco Nonella,[‡] Jürgen Schlitter,[†] Klaus Gerwert,[†] and Paul Tavan*[,‡]

Institut für Biophysik, ND04, Ruhr-Universität, 44780 Bochum, Germany, and Lehrstuhl für Biomolekulare Optik, Ludwig-Maximilians-Universität, Oettingenstrasse 67, 80538 München, Germany

Received: March 30, 2004; In Final Form: May 13, 2004

Due to the progress of density functional theory (DFT) accurate computations of vibrational spectra of isolated molecules have become a standard task in computational chemistry. This is not yet the case for solution spectra. To contribute to the exploration of corresponding computational procedures, here we suggest a more efficient variant of the so-called instantaneous normal-mode analysis (INMA). This variant applies conventional molecular dynamics (MD) simulations, which are based on nonpolarizable molecular mechanics (MM) force fields, to the rapid generation of a large ensemble of different solvation shells for a solute molecule. Short hybrid simulations, in which the solute is treated by DFT and the aqueous solvent by MM, start from snapshots of the MM solute−solvent MD trajectory and yield a set of statistically independent hydration shells partially adjusted to the DFT/MM force field. Within INMA, these shells are kept fixed at their 300 K structures, line spectra are calculated from the DFT/MM Hessians of the solute, and its inhomogeneously broadened solution spectra are derived by second-order statistics. As our test application we have selected the phosphate ions HPO_4^{2-} and $H_2PO_4^-$ because sizable solvation effects are expected for the IR spectra of these strongly polarizable ions. The widths, intensities, and spectral positions of the calculated bands are compared with experimental IR spectra recorded by us for the purpose of checking the computational procedures. These comparisons provide insights into the merits and limitations of the available DFT/MM approach to the prediction of IR spectra in the condensed phase.

1. Introduction

Whereas for molecules isolated in the vacuum highly accurate calculations of vibrational spectra have become simple and computationally manageable tasks due to the development[1,2] and widespread accessibility[3,4] of density functional theory (DFT) (see, e.g., refs 5−7), the computation of solution spectra is by no means simple nor standard. Here the question, which computational procedures are adequate, is the subject of a current debate.[8−11]

In principle, accurate descriptions of IR solution spectra have become accessible with the recent progress of hybrid methods (see ref 8 for an overview), whose key ideas were suggested about three decades ago by Warshel and Levitt.[12] Here, the solute molecule is treated quantum mechanically by DFT and is called the DFT fragment of the simulation system. The solvent environment is microscopically modeled by a conventional nonpolarizable molecular mechanics (MM) force field (see, e.g., ref 13) and, therefore, is called the MM fragment. The DFT/MM hybrid force field approximately accounts for the interactions between the two fragments. It includes the electrostatic polarizability of the solute through DFT and neglects that of the solvent beyond the mean field approximation, on which nonpolarizable MM force fields generally rely (see refs 14−16 for critical discussions). For a phosphate ion in aqueous solution, Figure 1 (right) shows a part of such a DFT/MM simulation system and its partitioning into fragments.

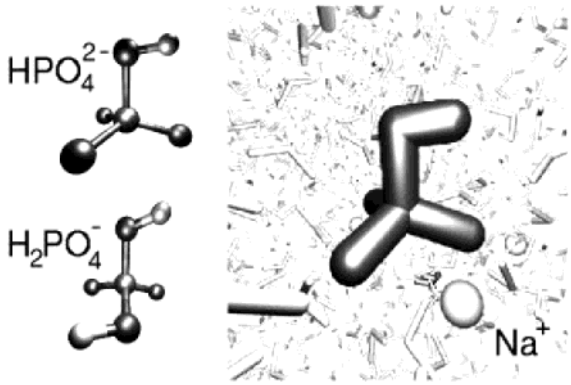

Figure 1. Left: Structures of the two phosphate ions HPO_4^{2-} and $H_2PO_4^-$ studied in this paper. Right: The ion HPO_4^{2-} (dark gray, DFT fragment) in aqueous solution (light gray, MM fragment).

Concerning the computation of vibrational spectra, the high quality of the particular DFT/MM hybrid approach suggested in ref 8 and implemented in the parallelized MD program EGO-MMII[17] has been previously demonstrated for DFT/MM models of the water dimer and for a DFT water molecule dissolved in MM water,[8] for the quinone cofactors (DFT) in a reaction center (MM) of bacterial photosynthesis,[18] and for *p*-benzoquinone (DFT) in MM water.[11] Note, however, that all these applications solely cover polar molecules in a similarly polar environment. In the case of ions, whose electrostatic interactions with a polar and polarizable environment are much stronger, the performance of the approach remains yet to be checked.

* Corresponding author: tavan@physik.uni-muenchen.de.
[†] Ruhr-Universität.
[‡] Ludwig-Maximilians-Universität.

10.1021/jp048617g CCC: $27.50
Published on Web 06/25/2004

DFT/MM hybrid MD simulations of solvent−solute systems enable the computation of vibrational spectra by Fourier transformation of time-correlation functions (FTTCF).[19] However, FTTCF requires extended MD trajectories and does not give easy access to the calculation of isotope effects.[11] Furthermore, it does not give the normal modes of the solute molecule, which are required for a detailed analysis of the force field (see ref 11 for further discussions).

To gain access also to the normal modes of a solute molecule in a DFT/MM setting, we will therefore apply the so-called instantaneous normal-mode analysis (INMA).[11] According to INMA various statistically independent snapshots are taken from an MD trajectory of the solute−solvent system, the Hessians of the solute are calculated within the snapshot ensemble of solvent cages, which are kept fixed at their 300 K structures, and the spectral positions, inhomogeneous widths, and intensities of the vibrational bands are derived from the average positions, spectral fluctuations, and transition dipole moments of the calculated vibrational lines. Finally, Gaussian models for the band shapes are used for the construction of an IR spectrum.

This INMA protocol deviates from the earlier suggestions of Eichinger[9] and Cui and Karplus,[10] according to which the solute−solvent snapshot geometries should be *jointly* optimized either by rapid freezing[9] or by energy minimization.[10] However, one can expect that the joint optimization of the solute−solvent structures strongly restricts the calculated ensemble of solvent cages. This ensemble will then mimic a low temperature and, therefore, should entail much too narrow bandwidths.

In ref 11 both FTTCF and the above INMA protocol have been applied to compute the IR spectra of *p*-benzoquinone in aqueous solution from a 17.5-ps DFT/MM hybrid MD trajectory. The spectral positions of the IR bands calculated by the two approaches turned out to agree quite well, demonstrating that both approaches are valid. In contrast, the bandwidths and IR intensities calculated by FTTCF and INMA showed marked differences, indicating that the 17.5-ps trajectory, although representing a huge computational effort, has been too short for a statistically reliable computation of these observables. For instance in the case of INMA, the requirement of the statistical independence of the snapshots and the known relaxation time of water at 300 K have enforced time delays of at least 2.5 ps between subsequent snapshots, which has limited the number of snapshots to only seven.[20] Furthermore, due to the lack of experimental data, a detailed evaluation of the merits and deficiencies of the two methods had to be postponed.

Therefore, as to proceed in the establishment of methods, it is the aim of this contribution to check whether INMA, when applied to a sufficiently large statistical ensemble of snapshots, can reliably predict the frequencies, inhomogeneous widths, and intensities of the IR bands for a solute molecule in a DFT/MM hybrid setting. To enable a rapid computation of a sufficiently large snapshot ensemble we will modify the procedure. Instead of using a costly DFT/MM hybrid MD simulation as in ref 11, we will apply computationally much cheaper MM simulations for the generation of statistically independent solvent shells. Very short hybrid MD trajectories starting at different MM configurations then yield the ensemble of solvent cages used for INMA.

The two monophosphates depicted in Figure 1 should represent sensitive and challenging test cases, because these highly polarizable ions should exhibit strong solvation effects in aqueous solution. Furthermore, from the standpoint of biochemistry, it is an important task to establish a computational approach to the IR spectra of phosphate ions, because derivatives such as ATP or GTP play prominent parts in bioenergetics and signal transduction and because FTIR techniques, when combined with vibrational analyses, can help in understanding these processes at a molecular level.[21−24]

We will complement our DFT/MM hybrid calculations on the two monophosphates in solution by FTIR measurements although the IR spectra of these ions have been repeatedly measured (see ref 25 for an overview). The experimental reinvestigation of the IR spectra serves to guarantee comparable thermodynamic conditions (temperature, density, and ion concentration) in the two approaches, to verify the assignment of the IR bands, and to enable quantitative checks with respect to the accuracy of the computational results.

Deviations between calculated and observed IR spectra may then be due to insufficiencies of the applied DFT method, to the inadequacy of the applied harmonic approximation, or to shortcomings of the MM model of the solvent. To distinguish these sources of possible deviations, we will first have to get an estimate on the quality of the harmonic DFT force field employed by us, which is provided by the program CPMD.[4] This program employs plane wave expansions for the construction of the Kohn−Sham MOs, implements the frozen core approximation through the use of pseudopotentials, and is integrated[8] into the MD program package EGO-MMII[17] to enable DFT/MM calculations. The DFT quality estimate has to be done in the conventional vacuum setting by comparisons with results of standard DFT methods implemented in GAUSSIAN98,[3] since the accuracy of the corresponding force fields is well-established[7] and since gas-phase spectra of the phosphate ions, which could provide an experimental reference, are unknown to us and hard to measure.

2. Methods

2.1. Choice of DFT Procedures. As mentioned above, there are no vibrational spectra available for the monophosphates HPO_4^{2-} and $H_2PO_4^-$ isolated in the gas phase. Therefore, the evaluation and calibration of the particular DFT method that we want to apply to the solution spectra of these molecules has to rely on vacuum calculations of well-established quality.

The very fact that Becke−Perdew DFT calculations[26,27] (BP86) can yield *unscaled harmonic force fields*, which accurately match the experimental, i.e., anharmonic vibrational spectra, has first been demonstrated for *p*-benzoquinone[5,28] and for the main group homonuclear diatomics.[29] These calculations have been carried out with extended Gaussian basis sets[3] comprising p and d polarization functions. Meanwhile the excellent agreement of unscaled harmonic frequencies from BP86 calculations with gas-phase vibrational spectra has been confirmed for a large number of polyatomic molecules.[7] Here, the computation of anharmonic corrections has demonstrated that the agreement is caused by a fortunate cancellation of errors. This cancellation is inherent in BP86 and is lacking in other DFT methods, like, e.g., in Beckes three-parameter Lee−Yang−Parr (B3LYP) approach,[30,31] which should be a superior method according to theoretical considerations. Only after the inclusion of anharmonic corrections do the B3LYP fundamentals agree better with the observed spectra than the BP86 fundamentals.[7] But as compared to the harmonic BP86 frequencies, this improvement is very small. Therefore, BP86 is the DFT functional of choice for the computation of vibrational spectra, whenever one is forced to stick to the harmonic approximation for reasons of computational feasibility.

Having fixed the DFT functional to BP86, suitable basis sets remain to be determined. Due to the strong polarizability of

the phosphate group we will use for the all-electron calculations with Gaussian basis functions a most expensive 6-311++G** basis set,[3] which includes 3d and 1f functions on the heavy atoms and 2p and 1d functions on the hydrogens, and adds diffuse functions on both. The corresponding results will serve as a reference for the evaluation of the quality of the basis sets and of the pseudopotentials used by us in the plane-wave DFT program CPMD.[4]

INMA requires the consideration of many solvent cages, within which the energies of the phosphates have to be minimized and their Hessians have to be calculated. To keep these computations manageable, the size of the plane wave basis set should be at the lower limit compatible with the necessary accuracy. In this respect a series of test calculations has demonstrated (data not shown) that in combination with the BP86 functional the pseudopotentials suggested by Hartwigsen et al.[32] yield a satisfactory accuracy at sufficiently small basis sets. The corresponding plane-wave cutoff and the extension of the box, in which the charge density is calculated on a grid, have been determined by gradual decreases of the cutoff and box sizes until the energies of the phosphates started to sizably change. The result was a cutoff at 80 Ry corresponding to 22 716 plane waves and a minimal distance between any DFT atom and the surface of the box at 2.7 Å. We denote this DFT method by HGH/BP and the corresponding DFT/MM hybrid approach by (HGH/BP)/MM.

2.2. Simulation System and MM Force Field. For the computation of the IR solution spectra of the monophosphates two periodic boxes (46.6 $Å^3$) were filled with 3375 water molecules and eight HPO_4^{2-} or $H_2PO_4^-$ ions, respectively. Appropriate numbers of Na^+ ions were added to balance the negative charges. These compositions represent concentrations of 130 mM, which are close to the phosphate concentrations used in the FTIR experiments. At 300 K the densities of the solutions correspond to the experimental density of water at this temperature.

The water molecules have been treated by MM and described by a variant of the simple TIP3P (three-point transferable intermolecular potential) force field, in which, in contrast to the original TIP3P model,[33] the water molecules are completely flexible. The required force constants, partial charges, and Lennard-Jones parameters have been taken from the CHARMM19 force field.[34,35]

To ensure a close matching between the descriptions of the phosphates in the envisaged MM and (HGH/BP)/MM simulations, respectively, a CHARMM22-type[13] MM force field has been constructed for these ions as follows. First, vacuum HGH/BP calculations were executed for the two ions, through which equilibrium geometries and Hessian matrices were obtained. The parameters of the harmonic contributions to the force field (cf. Appendix) were derived from the equilibrium structures and through transformations of the Hessians into a basis of the relevant internal degrees of freedom. The parameters of the torsional potentials were derived from fits to the corresponding HGH/BP potential curves. Further details and the results are given in the Appendix, which also addresses the choice of Lennard-Jones parameters required both in the MM and in the (HGH/BP)/MM settings. The vacuum HGH/BP calculations yielded a set of ESP charges (see, e.g., ref 8 for details), which were used as initial guesses for the MM partial charges in setting up the simulation system. Improved estimates were then obtained by MD simulations based on the (HGH/BP)/MM Hamiltonian as described below.

2.3. MD Simulations. To determine the solvation effects on the structures and charge distributions of the phosphate ions and to obtain solution-adapted partial charges for their MM models, the freshly generated ionic solutions have been equilibrated first for 100 ps in the MM setting (using the vacuum estimates for the phosphate partial charges). Here, as in all other MM simulations, a time step of 1 fs and an NVT ensemble were used; the temperature was controlled through coupling to an external heat bath[36] (coupling time constant $\tau = 0.1$ ps, target temperature $T_0 = 300$ K). In contrast, in the (HGH/BP)/MM simulations the time step was reduced to 0.25 fs. In both settings the long-range Coulomb interactions were treated by the multiple moving-boundary reaction field approach of Mathias et al.[37] with a dielectric boundary toward a solvent continuum 23 Å distant from each molecule. Within that boundary the electrostatics was treated explicitly with use of the structure-adapted multipole method.[38,39] Here, the Coulomb sum was employed for the atomic partial charges up to a distance of 10 Å. Beyond this distance the electrostatics was computed by multipole expansions of the partial charge distributions within the water molecules and ions. The field, including the reaction field correction, generated by the environment of a respective DFT fragment was imported into the DFT Hamiltonian. For further details on the DFT/MM interface we refer to ref 8.

After the initial MM equilibrations the simulations were continued for another 100 ps serving to generate different initial conditions for a series of 0.1-ps (HGH/BP)/MM simulations. In each of these simulations one of the phosphate ions was selected as the DFT fragment. The calculated ESP charges were averaged over all hybrid trajectories and over equivalent atoms, i.e., the atoms of the different types P, O, O_H, and H, respectively, occurring in the phosphates (cf. Appendix). The thus obtained values have been taken as refined estimates for the MM partial charges of the phosphate ions in solution. Table 1 in Section 3 lists the values of the corresponding solvent-adapted partial charges. The hybrid simulations were also used for statistics over other structural parameters of the phosphates, for instance for the computation of the average bond lengths, which will be mentioned in Section 3.

By using the MM force field with the solvent-adapted partial charges for the phosphates the simulation systems were equilibrated at 300 K for another 100 ps. Subsequently, MD simulations with durations of 300 ps were carried out to produce the desired ensembles of independent solvent cages. Starting for each ionic species from three snapshots (at 100, 200, and 300 ps) of the corresponding simulations system, short 75-fs (HGH/BP)/MM simulations were executed for each of the eight solvated phosphates yielding a total of 24 different solvent configurations per species surrounding the respective DFT fragments.

2.4. INMA Calculations of IR Spectra. For each of the two ionic species and each of the 24 corresponding snapshots, the solvent cages were now kept fixed and the (HGH/BP)/MM Hamiltonian was minimized by gradient descent with respect to the coordinates of the DFT fragment until a local minimum was reached as detected by energy gradients smaller than 8.4×10^{-5} au. Next, the Hessian and the dipole gradients of the phosphates were calculated in the (HGH/BP)/MM setting. Here, analytical first derivatives and numerical second derivatives were used. These data served as inputs for normal-mode analyses executed in the usual way yielding normal modes, corresponding frequencies, and IR intensities for each snapshot. The normal modes were classified by visual inspection, and, separately in

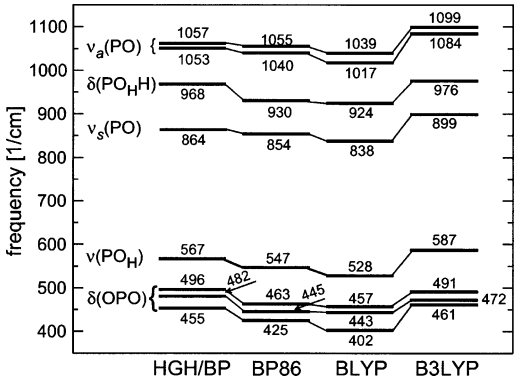

Figure 2. Frequencies of normal modes calculated by various DFT methods for HPO_4^{2-} isolated in a vacuum. Results of the HGH/BP approach provided by CPMD[4] are compared with results obtained from the BP86, BLYP, and B3LYP functionals implemented in GAUSSIAN98[3] (see Section 2 for computational details and the text for discussion).

each class, second order statistics was applied to the frequencies and intensities. With use of the standard deviations and average frequencies as parameters of normal distributions, the inhomogeneously broadened shapes and spectral positions of the various IR bands were obtained. After weighting these normalized Gaussians with the respective average intensities, they were added up to give the desired INMA IR spectra that can be directly compared with the observed IR spectra after proper adjustment of the intensity scale.

2.5. Experimental IR Spectra. The IR spectra of solvated K_2HPO_4 and KH_2PO_4 and of deuterated and ^{18}O-labeled phosphates have been measured at 300 K via FTIR. The FTIR measurements have been performed on a Bruker IFS 66/v spectrometer, using a DTGS detector and ZnSe windows. Spectra have been recorded with a spectral resolution of 4 cm^{-1} in the frequency range between 480 and 1300 cm^{-1} and have been apodized with the Blackman−Harris three-term function.[40] A zero-filling factor of 2 has been used. All samples consisted of $\sim$1 μm thick films of 100 mM solutions. Absorbance spectra have been calculated by means of a reference spectrum of pure H_2O (D_2O). K_2HPO_4 (99%) and KH_2PO_4 (99%) have been obtained from Merck and Baker, respectively, and have been measured without further purification. K_2DPO_4 and KD_2PO_4 have been prepared by drying the solution three times and rehydrating it with D_2O (99.9%, Deutero). ^{18}O-labeled phosphates have been synthesized by hydrolysis of PCl_5 (98%, Fluka) with $H_2{}^{18}O$ (99.1%, Isotec). Excess $H_2{}^{18}O$ has been removed by drying and rehydrating with H_2O. The pH value has been calibrated by HCl and NaOH. The HPO_4^{2-} and $H_2PO_4^-$ ions have been measured at pH 9.2 and 5.2. At pH 7.2 the two ions are found at a 1:1 ratio.

3. Results and Discussion

3.1. Checks of the HGH/BP Approach. We start with the required estimate on the quality of the DFT approach used by us, that is of HGH/BP. Figure 2 compares the gas-phase vibrational spectrum predicted for the doubly charged phosphate anion HPO_4^{2-} by the HGH/BP approach with results of DFT calculations obtained with the GAUSSIAN98 standard functionals BP86, BLYP, and B3LYP, respectively. For this comparison, as for all other comparisons below, we have chosen the spectral range above 400 cm^{-1}, because the transmission properties of the ZnSe windows set a corresponding lower limit to our FTIR spectra, and below 1300 cm^{-1}, because all vibrational modes involving motions of the heavy atoms have frequencies below this limit.[25]

All DFT methods agree that the frequencies of eight of the twelve normal modes of HPO_4^{2-} should be located in this range. These modes cover four different bond stretches ν between the heavy atoms P and O and four deformations δ of the angles between these atoms. For a more detailed characterization of the normal modes two properties of HPO_4^{2-} can be used. (i) There are two different oxygen bonding patterns, i.e., three oxygens are exclusively bound to P and one oxygen is additionally bound to the hydrogen (cf. Figure 1, top left). Therefore, the oxygens can be distinguished by introducing the atom types O and O_H, respectively. (ii) Due to the presence of three equivalent oxygens, the normal modes will comprise in-phase and out-of-phase combinations of the internal coordinates involving these oxygens. Therefore, they can be distinguished by the labels *s* and *a*, respectively. In Figure 2 the thus defined nomenclature has been used to classify the energy levels in the depicted term scheme. For instance, $\nu_s(PO)$ characterizes the normal mode, in which all three P−O bonds are simultaneously elongated or compressed.

Figure 2 shows that HGH/BP predicts frequencies that are upshifted by 23 cm^{-1} in a close to uniform fashion as compared to the BP86 reference. Therefore, the respective spectral orderings are identical. Identical orderings are also predicted by BLYP and B3LYP. Compared to BP86, these spectra show either an average red-shift by 11 cm^{-1} (BLYP) or an average blue-shift by 39 cm^{-1} (B3LYP). Thus, the harmonic HGH/BP force field is a little stiffer than that of the reference method BP86 (but softer than that of B3LYP) demonstrating that the use of pseudopotentials and of different basis sets is of minor importance. The consideration of our corresponding results for the other phosphate ion $H_2PO_4^-$ provides no further insights and, therefore, is omitted. Note, in addition, that refs 18 and 11 arrived at similar conclusions for a different class of molecules, i.e., the quinones, concerning the comparable qualities of Becke−Perdew DFT descriptions using GAUSSIAN98 and CPMD, respectively.

In view of the known quality of the harmonic BP86 force field in describing gas-phase spectra,[7] we thus conclude that the predictions of the closely related HGH/BP method also can be considered as high-quality estimates for the unknown gas-phase spectra of phosphate ions. Therefore, the effects of solvation on the structure and vibrational spectra of phosphate ions can be judged by comparison of HGH/BP vacuum results with experimental solution data.

3.2. Solvation Effects on the Phosphate Structures. In our MM simulations of the ionic solutions, the ions stayed away from each other as to maximize their hydration shells. The average distance of a sodium ion to the next phosphate was about 8 Å and never got smaller than 4 Å. Due to the strong dielectric shielding of the Na^+ charges by the surrounding water, the solvation effects, which are predicted by our (HGH/BP)/MM simulations for the phosphate ions, should be mainly due to their hydration shells, whereas the influence of the sodium ions should be small.

We first turn to the hydration-induced changes of the charge distributions within the phosphate ions. As observables we use the electrostatic potential (ESP) partial charges derived from the HGH/BP vacuum calculations and from the (HGH/BP)/MM solvent simulations described in Section 2. These charges are optimized so as to match the electrostatic potential generated by a molecule at its van der Waals surface. Table 1 lists the resulting partial charges for the two phosphate ions under

TABLE 1: ESP Partial Charges *q* Given in Units of the Elementary Charge e for HPO_4^{2-} and $H_2PO_4^-$ in a Vacuum and in Solution, Respectively, As Derived from HGH/BP and (HGH/BP)/MM Calculations[a]

	HPO_4^{2-}		$H_2PO_4^-$	
atom type	vacuum	solution	vacuum	solution
P	+1.71	+1.43	+1.26	+1.20
O	−1.05	−1.02	−0.79	−0.86
O_H	−0.87	−0.76	−0.68	−0.64
H	+0.31	+0.39	+0.34	+0.40

[a] The solution values represent averages over a series of short (HGH/BP)/MM trajectories (see Section 2 for details and the Appendix for the definition of the atom types).

consideration. The partial charges in solution represent averages over the ensembles of 24 short (HGH/BP)/MM simulations described in Section 2. The fluctuations of the partial charges are very small as documented by the average standard deviations of 0.03 e. For both ions an analysis of the data reveals that the hydration shifts about 30% of the negative charge, which in vacuo is located at the O_H-H groups, toward the PO_3 and PO_2 moieties of HPO_4^{2-} and $H_2PO_4^-$, respectively. These substantial charge shifts are convincing witnesses for the strong polarizabilities of the phosphate ions.

The shifts of charge density are accompanied by hydration-induced decreases of the $P-O_H$ bond lengths (from 1.78 Å to an average value of 1.67 Å for HPO_4^{2-} and from 1.67 Å to an average value of 1.63 Å for $H_2PO_4^-$). According to the usual arguments, the shortening of a bond length points toward an increase of the corresponding bond stretching force constant. Therefore, one expects strong blue-shifts for the frequencies of all normal modes, to which the $P-O_H$ bond stretch gives an important contribution. For the case of the HPO_4^{2-} ion, whose vacuum spectrum has been discussed above in connection with Figure 2, we therefore expect that the modes $\nu(PO_H)$ and $\delta(PO_HH)$ will be strongly blue-shifted by hydration.

3.3. Assignment of FTIR Bands by INMA Results. Figure 3 compares the IR spectra of HPO_4^{2-} (a, b) and $H_2PO_4^-$ (c, d) as measured by FTIR (a, c) with the results of the INMA (b, d) calculations.

The FTIR spectrum of HPO_4^{2-} depicted in Figure 3a exhibits four rather sharp peaks a−d at 1080, 990, 855, and 541 cm^{-1}, respectively, as well as a very weak and broad shoulder s. Baril et al.[25] have attributed this shoulder, which was also visible in their IR spectra, to a band at 1197 cm^{-1}. Likewise the corresponding INMA spectrum shown in Figure 3b predicts four sharp bands, one of them being generated by two out-of-phase P−O stretching modes $\nu_a(PO)$, and a very broad band, which is due to the $P-O_H-H$ bending mode $\delta(PO_HH)$.

If one takes the calculated shapes and relative intensities of the INMA bands as a guideline and if one assumes that our (HGH/BP)/MM approach correctly reproduces the spectral ordering of the *sharp* peaks, then the visual comparison of the FTIR and INMA spectra in parts a and b of Figure 3 immediately suggests an assignment of the FTIR peaks. In particular, the most intense and high-frequency peak a has to be assigned to a superposition of the two intense INMA bands $\nu_a(PO)$, the less intense peak b to the equally less intense INMA band $\nu_s(PO)$ associated with the in-phase P−O stretch, the broader peak c to the broader INMA band $\nu(PO_H)$, and peak **d** to the three neighboring INMA bands $\delta(OPO)$. Thus, in the FTIR spectrum of Figure 3a only the weak shoulder s at 1197 cm^{-1} remains to be assigned and, here, the very broad INMA band $\delta(PO_HH)$ of the $P-O_H-H$ bending mode is the only remaining candidate. Note that the latter suggestion agrees with an earlier assignment.[25]

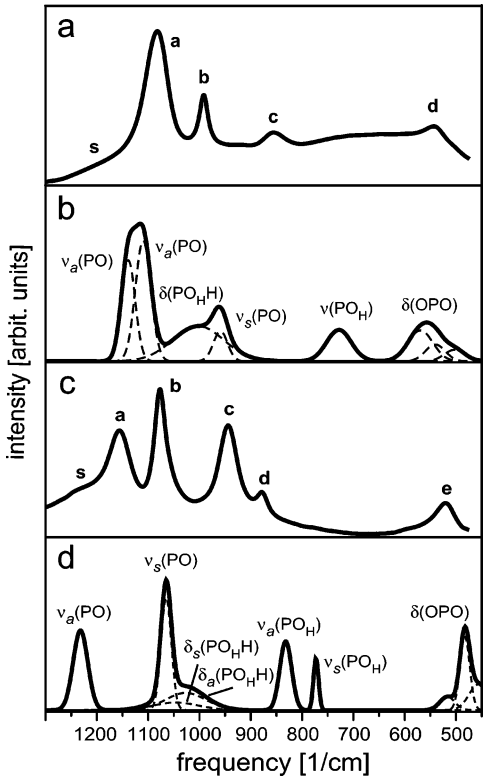

Figure 3. Comparison of the IR spectra obtained for HPO_4^{2-} (a, b) and $H_2PO_4^-$ (c, d) by FTIR (a, c) and INMA (b, d), respectively. For computational and experimental details see Section 2 and for a discussion see the text.

The above assignment of the FTIR spectrum of HPO_4^{2-} in aqueous solution has been based on the intensities, the band shapes, and the spectral ordering of the sharp bands predicted by the INMA calculations. Somewhat surprisingly it implies that the (HGH/BP)/MM approach has severe deficiencies concerning the description of band frequencies, because the spectral positions of several INMA bands in Figure 3b sizably deviate from those of their FTIR counterparts in Figure 3a. Therefore we should check as to whether similar deficiencies appear also in the related case of the singly charged anion $H_2PO_4^-$.

The FTIR spectrum of $H_2PO_4^-$ depicted in Figure 3c exhibits five sharp bands a−e at 1156, 1077, 944, 879, and 521 cm^{-1}, respectively, and a broad shoulder s at 1213 cm^{-1}. Also the corresponding INMA spectrum in Figure 3d shows one broad and five sharp bands. Applying once again the criteria explained above, the FTIR peak a is assigned to $\nu_a(PO)$, peak b to $\nu_s(PO)$, peaks c and d to the two $P-O_H$ stretches $\nu_a(PO_H)$ and $\nu_s(PO_H)$, respectively, and peak e to the assembly of O−P−O bending modes surrounding the sharp $\delta(OPO)$ band predicted by INMA at 483 cm^{-1}. In agreement with an earlier suggestion,[25] finally the broad FTIR shoulder at 1213 cm^{-1} has to be assigned to the two $P-O_H-H$ bending modes generating the broad INMA bands $\delta_s(PO_HH)$ and $\delta_a(PO_HH)$.

Having tentatively assigned the IR bands also for $H_2PO_4^-$, a comparison of the spectral positions of corresponding bands in Figure 3c,d now strengthens the suspicion that the (HGH/BP)/MM approach cannot predict the vibrational frequencies of small ions in aqueous solution at the same level of accuracy at which pure DFT treatments such as HGH/BP usually describe the gas-

phase spectra of a wide class of molecules.[7] Also for $H_2PO_4^-$ some of the FTIR frequencies strongly deviate from the INMA results.

Because this conclusion depends on the correctness of the assignments, we will now shortly discuss isotope effects for clarification. To save space we will not show the corresponding FTIR and INMA spectra (see, however, the Supporting Information for some of these spectra). Instead we will merely infer the key results.

3.4. Corroboration of Assignment by Isotope Labeling. The most intense FTIR band a at 1080 cm^{-1} of HPO_4^{2-} (cf. Figure 3a) splits in D_2O into two bands at 1097 and 1079 cm^{-1}, respectively. This observation proves two aspects of our assignment. The splitting demonstrates that the HPO_4^{2-} band a is actually due to two nearly degenerate P−O stretching modes ν_a(PO) described by INMA. The 17-cm^{-1} blue-shift induced by deuteration at one of the ν_a(PO) modes shows that another mode, which in H_2O is coupled to this ν_a(PO) mode and is located at a higher frequency, must have been strongly red-shifted and correspondingly decoupled upon deuteration. According to our assignment this higher frequency mode should be the $\delta(PO_HH)$ vibration, which we have associated to the very weak shoulder at 1197 cm^{-1}.

The INMA results on DPO_4^{2-} corroborate this analysis. As main effects of deuteration they predict a large 269-cm^{-1} red-shift for $\delta(PO_HH)$, which decouples this local mode from one of the nearby ν_a(PO) modes, and a sizable 18-cm^{-1} red-shift for this ν_a(PO) mode, proving the decoupling. In this context it is irrelevant that INMA assigns the wrong sign to the decoupling shift of ν_a(PO). Because INMA has erroneously located the $\delta(PO_HH)$ frequency *below* that of ν_a(PO), the wrong sign of the calculated decoupling shift of ν_a(PO) is a necessary consequence. The FTIR spectrum of DPO_4^{2-} furthermore reveals that the peak c of the HPO_4^{2-} spectrum in Figure 3a is red-shifted by 20 cm^{-1}. INMA predicts for the corresponding $\nu(PO_H)$ mode a similar deuteration shift of 14 cm^{-1}.

For HPO_4^{2-} the decoupling argument is our key indication on the spectral location of $\delta(PO_HH)$ at 1197 cm^{-1}. As is apparent from Figure 3a, the weak intensity in the 1200-cm^{-1} spectral range prevents the clear-cut and direct identification of this $\delta(PO_HH)$ band, which according to INMA should be very broad. Due to baseline problems in the D_2O spectrum, we were also unable to detect the expected disappearance of the weak shoulder from the 1197-cm^{-1} spectral location.

For $H_2PO_4^-$, however, the experimental evidence for the location of the corresponding $\delta(PO_HH)$ bands at the blue edge of the spectral range is direct. Here, the broad shoulder at 1213 cm^{-1} is more intense (cf. Figure 3c) and this shoulder clearly disappears upon deuteration. Quite like in the case of HPO_4^{2-}, the FTIR spectrum of $D_2PO_4^-$ also reveals a deuteration-induced decoupling of the ν_a(PO) mode from the higher frequency $\delta(PO_HH)$ modes as witnessed by a 21-cm^{-1} blue-shift of the ν_a(PO) band a in D_2O. Because of the additional direct spectroscopic evidence on the high-frequency location of the $\delta(PO_HH)$ modes, the decoupling argument can thus be considered as hard evidence also for HPO_4^{2-} and finally proves the assignment of the very weak shoulder in Figure 3a to $\delta(PO_HH)$.

Also for $H_2PO_4^-$ the decoupling is described by INMA. The deuteration shifts the frequency of the ν_a(PO) mode by 20 cm^{-1} to the red, because the $\delta(PO_HH)$ modes are shifted by about 300 cm^{-1} to much lower frequencies. Again the sign of the 20 cm^{-1} decoupling shift is wrong, because the $\delta(PO_HH)$ frequencies are underestimated. Finally, the observed 17-cm^{-1} red-shift of band d is nicely reproduced by INMA predicting a 22-cm^{-1} red-shift of the associated $\nu(PO_H)$ band.

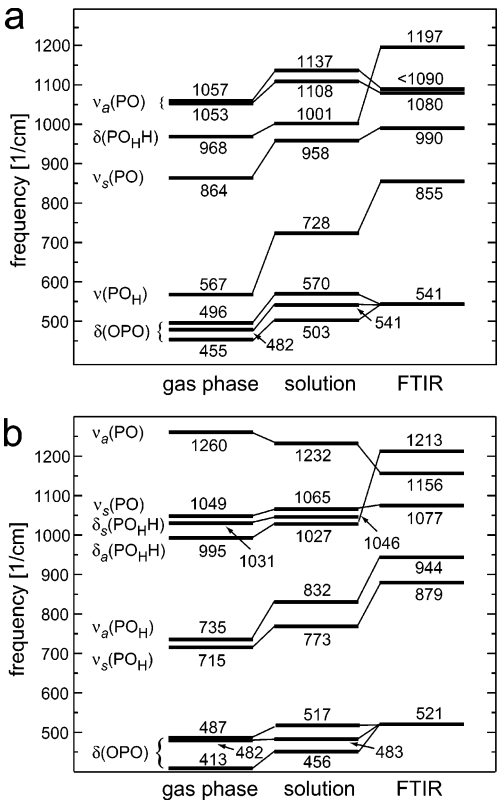

Figure 4. Hydration effects on the vibrational spectra (a) of HPO_4^{2-} and (b) of $H_2PO_4^-$. The gas-phase frequencies calculated by HGH/BP are compared with the average INMA frequencies obtained by (HGH/BP)/MM for the solution case and with the band positions measured by FTIR. For a discussion see the text.

Apart from corroborating for both ions the assignments of the sharp FTIR peaks in the 800−1300 cm^{-1} range to P−O and P−O_H stretching vibrations, the substitution of the oxygens by ^{18}O isotopes does not add any further insights. On the average these peaks experience 33-cm^{-1} red-shifts. In nice agreement INMA predicts an average red-shift of 35 cm^{-1} for the corresponding modes.

3.5. Hydration Effects on Vibrational Frequencies. Having fixed the assignment of all IR bands in the 400−1300 cm^{-1} spectral range we are now prepared to answer the questions (i) as to how the spectral locations of the various vibrational modes are modified by hydration and (ii) to what extent these effects are covered by our (HGH/BP)/MM approach.The answers are provided by the two-term schemes in Figure 4, which compare for the two phosphate ions the gas-phase spectra estimated by vacuum HGH/BP calculations (first columns) with the spectral locations of the IR bands observed in solution (last columns) and with their INMA descriptions (central columns). Because of the established quality of our DFT method (cf. Section 3.1), the HGH/BP estimates of the unknown gas-phase spectra should be accurate within a few wavenumbers. Therefore, the comparisons of these estimates with the FTIR solution spectra can provide insights into the effects of hydration.

Already a first glance at the two-term schemes in Figure 4 reveals that hydration causes very large shifts of the vibrational frequencies by at least 25 cm^{-1} up to as much as 288 cm^{-1} (compare the first and last columns). With the sole exception of ν_a(PO) in $H_2PO_4^-$, all frequencies are shifted to the blue. The hydration effects are particularly pronounced for all modes, which involve motions of the protonated oxygen atoms O_H.

Here, the $P-O_H$ stretches experience blue-shifts on the average by 220 cm^{-1} and the $P-O_H-H$ bending vibrations by 165 cm^{-1}. Recall that our analysis of the hydration effects on the phosphate structures (cf. Section 3.2) had led us to expect the former blue-shifts. In line with these arguments, the unusual magnitude of these shifts is a signature of the large polarizability of the phosphate ions and of the strong polarity of the aqueous solvent. As a result, the vibrational spectra of the phosphate ions represent a particularly hard testing case for any method, which is supposed to describe the vibrational spectra of molecules in polar solvents.

To apply this test to our (HGH/BP)/MM hybrid method, we compare the central columns of the term schemes in Figure 4 with the gas-phase and FTIR solution spectra in the neighboring columns. Apart from two apparent exceptions to be discussed further below, the inclusion of the MM solvent into the DFT description shifts all vibrational levels from their gas-phase positions toward the FTIR solution values. However, as seen most clearly at the blue-shift of the $P-O_H$ stretching mode of HPO_4^{2-}, this approach toward the FTIR spectrum covers only about half the distance: The (HGH/BP)/MM treatment shifts the frequency of $\nu(PO_H)$ only by 161 cm^{-1} to the blue of the HGH/BP vacuum result instead of the 288 cm^{-1} required by FTIR.

The only exceptions from this general trend apparent in the term schemes are the large blue-shifts of the two ν_a(PO) modes of HPO_4^{2-}, which exceed the required 25-cm^{-1} shifts on the average by about 40 cm^{-1}. But these exceptions are easily understood in terms of the coupling between the corresponding local ν_a(PO) modes and the local $\delta(PO_HH)$ mode analyzed in Section 3.4. The (HGH/BP)/MM modeling of the hydration apparently does not suffice to shift the intrinsic frequency of the local $\delta(PO_HH)$ mode above those of the local ν_a(PO) modes as required by FTIR. Therefore, in INMA the coupling between these local modes induces a spectral splitting, which shifts the ν_a(PO) frequencies too far to the blue and diminishes the blue-shift of $\delta(PO_HH)$ by the same amount.

Note here that the absolute value predicted by (HGH/BP)/MM for this spectral splitting is about as large ($\approx$100 cm) as the one found by FTIR. When taken together with the fact that the deuteration effects have revealed similarly sized couplings in both cases, the comparable magnitudes and the opposite signs of the splittings show that the intrinsic frequency of the local $\delta(PO_HH)$ mode must be located experimentally just above and, according to the (HGH/BP)/MM description, just below those of the two local ν_a(PO) modes. Similar coupling effects between the local ν_a(PO) mode and the two local $\delta(PO_HH)$ modes can be deduced from Figure 4b also for $H2PO_4^-$. In this case, however, they do not disturb the homogeneity by which the vibrational levels approach the FTIR spectra upon inclusion of an MM solvent model into the DFT description of the phosphate.

In summary, the (HG/BP)/MM treatment of the two phosphate ions in aqueous solution can qualitatively account for the effects of hydration on the vibrational spectra, but it underestimates these effects by about a factor of 2. The hydration effects are particularly large for all modes involving the motions of a protonated oxygen atom, that is for the $P-O_H$ stretching and $P-O_H-H$ bending vibrations. Therefore, the deviations of the (HG/BP)/MM frequencies from the FTIR observations are particularly large for these modes. In the case of the $P-O_H-H$ bending vibrations, hydration shifts the frequencies according to FTIR to the blue edge of the investigated spectral range. Here, the (HG/BP)/MM underestimate of hydration effects even causes a wrong spectral ordering.

3.6. Inhomogeneous Bandwidths and Intensities. In Section 3.3 we have assigned the FTIR bands to normal modes by visually comparing the INMA band shapes and intensities with corresponding features of the FTIR spectra. Apart from the assumption that INMA predicts a correct spectral ordering for the sharp bands, we have largely ignored the detailed spectral positions of the bands in this process. Its apparent success demonstrates that INMA performs quite well on the shapes and relative intensities of the IR bands.

Unfortunately the insufficient quality of our FTIR spectra prevents for many bands a quantitative comparison of their widths and intensities with the INMA descriptions. Solely for the three high-frequency FTIR bands s, a, and b of $H_2PO_4^-$ (cf. Figure 3c), a reasonable Gaussian fit was possible. This fit yielded bandwidths of 114, 46, and 26 cm^{-1}, respectively. The INMA values are 99, 33, and 24 cm^{-1}, respectively, for the corresponding bands associated with the two $\delta(PO_HH)$, the ν_a(PO) and ν_s(PO) modes. Thus, on the average, INMA underestimates the FTIR bandwidths only by 17% and we may conclude that the INMA procedure of sampling different hydration cages can reasonably account for the fluctuations of the electric field, by which the strong electrostatic dipoles of the thermally moving water molecules polarize the phosphate ions.

As quantitatively determined here and as is apparent from the INMA results in Figure 3b,d, the $\delta(PO_HH)$ bands are much broader than the other bands. This large broadening is readily understood by considering the fact that the $P-O_H-H$ bending modes involve the motion of a single proton, whereas all other modes exclusively comprise heavy nuclei. Therefore, the charge density localized by the weak Coulomb potential of the proton and associated with the O_H-H bond is much more strongly perturbed by the fluctuations of the external electric field than the charge densities of the P−O and $P-O_H$ bonds. In Section 3.2, we have already noted another signature of this effect, that is the hydration-induced charge transfer from the peripheral O_H-H group toward the core of the molecule.

Concerning the accuracy of the calculated relative intensities the above fit renders only two numbers and, therefore, one cannot derive any further conclusions. In this respect we have to be content with the positive judgment on the corresponding performance of INMA stated above.

4. Discussion and Outlook

Apart from small underestimates, our computationally more efficient INMA protocol turned out to reproduce the widths of the phosphate IR bands quite well. This result proves that the sampled ensemble of hydration shells appropriately covers the fluctuations of the electric field, by which the surrounding water dipoles polarize the phosphate ions. Also the IR intensities calculated by INMA seem to be reasonable. In line with the arguments in ref 11 this finding demonstrates that the neglect of the kinetic couplings between the solute and the solvent, which is a characteristic of the INMA approach, hardly affects the intensities. However, the hydration effects on the spectral locations of the phosphate IR bands predicted by our DFT/MM Hamiltonian turned out to be underestimated by about a factor of 2, and this result requires an explanation.

In Section 3.1 we have demonstrated that the DFT part of the hybrid Hamiltonian, that is the HGH/BP method provided by CPMD, is as accurate as standard high-quality DFT methods: Despite the applied harmonic approximation the calculated IR spectra should therefore deviate from corresponding observations only by a few wavenumbers per band.

TABLE 2: Parameters of the Bonded Force Field 1 for the Phosphate Ions[a]

ij	f_{ij}	$r_{0,ij}$, Å
O−P	395	1.61
O_H−P	98	1.87
O_H−H	519	0.98
ijk	f_{ijk}	$\varphi_{0,ijk}$, deg
O−P−O	73	116
O−P−O_H	73	105
P−O_H−H	45	105
ijkl	k_{ijkl}	δ_{ijkl}, deg
O−P−O_H−H	0.6	180

[a] The force constants f_{ij} of the bonds are given in kcal/(mol·Å^2), those of the angles (f_{ijk}) in kcal/(mol·deg^2), and the torsional barriers k_{ijkl} in kcal/mol. The phosphate atom types P, O, O_H, and H are explained in the text.

Correspondingly, the detected underestimate of the hydration effects must be due to insufficiencies of the MM part and, here, the most likely cause is the neglect of the electronic polarizability in the MM force field. The following arguments support this explanation.

Nonpolarizable MM force fields for water, like the one by which we try to cover the effects of hydration in our hybrid calculations, have been designed as mean field models for water molecules in a polar environment, that is in pure water (cf. the recent review in ref 14). In particular, the dipole moments of the MM water models are fixed at a value which exceeds that of an isolated water molecule by about 40%. As demonstrated by DFT and DFT/MM simulations,[8,41] in liquid water the dipole moments of the water molecules increase by about this percentage due to their polarization by surrounding water dipoles. As a result, the transferability of these MM water models into a different environment, like into the hydration shell of a small ion, is not guaranteed.[14]

A small ion generates a much stronger electric field than a water molecule. Therefore, the induced dipole moments of the water molecules in its hydration shell will be larger than those of water molecules, which are in the environment of pure liquid water. In particular, the resulting total dipole moments of the water molecules hydrating the ion will be larger than the fixed values provided by the MM force field. For a small ion, these arguments lead to the general expectation that the hydration effects, which are calculated from such a force field in a DFT/MM setting, will be sizably underestimated. Our results for the phosphate ions, in particular the nearly homogeneous but incomplete approach of the DFT/MM vibrational levels toward the FTIR solution values, support this expectation. Concurrently the above arguments also explain why this DFT/MM setting performs well[8,11] for polar molecules solvated in water. Here, the effects of polarizability resemble more closely those in pure water and the nonpolarizable MM force fields are more appropriate.

However, as correctly argued by both referees, also a charge transfer between the phosphate ions and the hydrating water molecules, which is unaccounted for by our simple DFT/MM approach confining the DFT description to the phosphates, could contribute to the noted underestimate of the hydration effects.

For a check of these hypotheses one should recalculate the vibrational spectra of the phosphate ions using a polarizable MM force field for the water and, in addition, more extended DFT fragments covering the first hydration shells of the phosphates. Here, the chosen MM_{pol} force field for the water molecules should closely model the properties, which are predicted for these molecules by the applied DFT functional. Such a parametrization will then enable a smooth transition from an initial MM_{pol} to a subsequent DFT description of the water molecules in the first hydration shells of the DFT phosphate ions. Finally, a comparison of the phosphate vibrational spectra resulting from these two sets of additional calculations will provide estimates on the relative sizes, by which the two effects neglected by us (polarizability vs charge transfer) can correct the descriptions. But whatever these future studies may show, our results have clearly demonstrated that the quantitatively correct DFT/MM description of the phosphate vibrational levels represents a hard and sensitive test for the quality of the chosen computational method and, here, particularly for the quality and transferability of polarizable MM force fields.

Acknowledgment. G.M. and M.N. acknowledge support by the Volkswagen-Stiftung (project I/73 224) and P.T. a grant by the Deutsche Forschungsgemeinschaft (SFB533/C3). The Bochum group is grateful for support by the Deutsche Forschungsgemeinschaft and to B. Portmann, C. Wegener, and F. Wennmohs for setting up the Myrinet linked PC cluster used for the calculations. The authors thank Matthias Schmitz for his careful proofreading of the manuscript.

Supporting Information Available: FTIR spectra of $H_2PO_4^-$ and of the isotopomers $D_2PO_4^-$ and $H_2P^{18}O_4^-$ (Figure S1) as well as a band fit to the FTIR spectrum of $H_2PO_4^-$ (Figure S2). This material is available free of charge via the Internet at http://pubs.acs.org.

Appendix: MM Phosphate Force Field

During the MM simulations the so-called "bonded" interactions within the phosphate ions were described by a model potential

$$E_{\mathrm{MM,bond}} = \sum_{ij} f\,(r - r_0)^2 + \sum_{ijk} f\,(\varphi - \varphi_0)^2 + \sum_{ijkl} (k/2)(1 + \cos(3\theta + \delta)) \quad (1)$$

which is based on the CHARMM22 concepts.[13] The indices run over all atoms, which are covalently connected through at most three chemical bonds. The variables r, φ, and θ characterize the associated internal coordinates (for simplicity the required indices have been omitted). The first term assigns a harmonic bond stretching potential to all covalently connected atom pairs. The harmonic potentials of the second term serve to keep the bond angles close to their equilibrium values, and the third term parametrizes the torsional potentials. Identical values are chosen for the force constants f, the torsional energy barriers k, the equilibrium bond lengths r_0, and angles φ_0, as well as for the phase shifts δ, if the atoms involved have identical atom types. In CHARMM22 atom types are assigned to all atoms of a molecule according to their respective covalent bonding patterns.

In the phosphate ions, four atom types are required for the classification of the atoms. These are the phosphorus P, the hydroxyl oxygens O_H, the remaining oxygens O, and the hydroxyl hydrogens H. Table 2 collects the parameters of the phosphate model potential 1, which have been determined by vacuum HGH/BP calculations as sketched in Section 2.

The Lennard-Jones parameters, which cover the van der Waals interactions in the simulation system both in the pure MM and in the hybrid DFT/MM settings, have been taken from the CHARMM22 file parallh22x.nuc by using the CHARMM22 atom types P for P, ON4 for O_H, ON3 for O, and HN4 for H.

Solution-adapted partial charges q_i calculated by (HGH/BP)/MM simulations (cf. Section 2) and required for pure MM simulations, are collected in Table 1.

The quality of the thus defined MM force field has been checked by the computation of the vacuum vibrational spectra. In the case of HPO_4^{2-}, for instance, we have obtained MM frequencies for the modes shown in Figure 2, which exhibit rms deviations of 55 cm^{-1} from the HGH/BP results and of 44 cm^{-1} from BP86, respectively, while preserving the energetic ordering of the modes. Since vibrational spectra are very sensitive to the details of a force field, this quite good agreement demonstrates that the MM parameters in Table 2 represent a reasonable choice.

References and Notes

(1) Hohenberg, P.; Kohn, W. *Phys. Rev. B* **1964**, *136*, 864−870.

(2) Kohn, W.; Sham, L. J. *Phys. Rev. A* **1965**, *140*, 1133−1138.

(3) Frisch, M. J.; Trucks, G. W.; Schlegel, H. B.; Scuseria, G. E.; Robb, M. A.; Cheeseman, J. R.; Zakrzewski, V. G.; Montgomery, J. A., Jr.; Stratmann, R. E.; Burant, J. C.; Dapprich, S.; Millam, J. M.; Daniels, A. D.; Kudin, K. N.; Strain, M. C.; Farkas, O.; Tomasi, J.; Barone, V.; Cossi, M.; Cammi, R.; Mennucci, B.; Pomelli, C.; Adamo, C.; Clifford, S.; Ochterski, J.; Petersson, G. A.; Ayala, P. Y.; Cui, Q.; Morokuma, K.; Malick, D. K.; Rabuck, A. D.; Raghavachari, K.; Foresman, J. B.; Cioslowski, J.; Ortiz, J. V.; Stefanov, B. B.; Liu, G.; Liashenko, A.; Piskorz, P.; Komaromi, I.; Gomperts, R.; Martin, R. L.; Fox, D. J.; Keith, T.; Al-Laham, M. A.; Peng, C. Y.; Nanayakkara, A.; Gonzalez, C.; Challacombe, M.; Gill, P. M. W.; Johnson, B. G.; Chen, W.; Wong, M. W.; Andres, J. L.; Head-Gordon, M.; Replogle, E. S.; Pople, J. A. Gaussian 98, revision A.5; Gaussian, Inc.: Pittsburgh, PA, 1999.

(4) Hutter, J.; Alavi, A.; Deutsch, T.; Bernasconi, M.; Goedecker, S.; Marx, D.; Tuckermann, T.; Parrinello, M. *CPMD*, Version 3.4.0; MPI für Festkörperforschung and IBM Zurich Research Laboratory.

(5) Nonella, M.; Tavan, P. *Chem. Phys.* **1995**, *199*, 19−32.

(6) Zhou, X.; Mole, S. J.; Liu, R. *Vib. Spectrosc.* **1996**, *12*, 73−79.

(7) Neugebauer, J.; Hess, B. A. *J. Chem. Phys.* **2003**, *118*, 7215−7225.

(8) Eichinger, M.; Tavan, P.; Hutter, J.; Parrinello, M. *J. Chem. Phys.* **1999**, *110*, 10452−10467.

(9) Eichinger, M. Thesis, Ludwig-Maximilians Universität München, Germany, 1999.

(10) Cui, Q.; Karplus, M. *J. Chem. Phys.* **2000**, *112*, 1133−1149.

(11) Nonella, M.; Mathias, G.; Tavan, P. *J. Phys. Chem. A* **2003**, *107*, 8638−8647.

(12) Warshel, A.; Levitt, M. *J. Mol. Biol.* **1976**, *103*, 227−249.

(13) MacKerell, A. D.; et al. *J. Phys. Chem.* **1998**, *102*, 3586−3616.

(14) Guillot, B. *J. Mol. Liquids* **2002**, *101*, 219−260.

(15) Ponder, J. W.; Case, D. A. *Adv. Protein Chem.* **2003**, *66*, 27−85.

(16) Tavan, P.; Carstens, H.; Mathias, G. Molecular dynamics simulations of proteins and peptides: Problems, achievements, and perspectives. In *Handbook of Protein Folding*; Buchner, J., Kiefhaber, T., Eds.; Wiley-VCH: Weinheim, Germany, 2004, in press.

(17) Mathias, G.; Eichinger, M.; Carstens, H.; Stork, M.; Weiss, A.; Heller, H.; Grubmüller, H.; Egwolf, B.; Niedermeier, C.; Tavan, P. *EGO-MMII users guide*; Lehrstuhl für BioMolekulare Optik, Ludwig Maximilian Universität München, Oettingenstrasse 67, D-80538 München, unpublished.

(18) Nonella, M.; Mathias, G.; Eichinger, M.; Tavan, P. *J. Phys. Chem. B* **2003**, *107*, 316−322.

(19) Allen, M. P.; Tildesley, D. J. *Computer Simulation of Liquids*; Oxford University Press: Oxford, UK, 1996.

(20) Computational limitations have enforced a similarly bad statistic (10 snapshots) in the INMA calculations of Cui and Karplus.[10]

(21) Gerwert, K. Molecular Reaction Mechanism of Proteins Monitored by Time-resolved FT-IR Difference Spectroscopy. In *Handbook of Vibrational Spectroscopy*; Chalmers, J. M., Griffiths, P. R., Eds.; John Wiley: Chichester, UK, 2001; Vol. 5.

(22) Cepus, V.; Goody, R. S.; Scheidig, A. J.; Gerwert, K. *Biochemistry* **1998**, *37*, 10263−10271.

(23) Allin, C.; Gerwert, K. *Biochemistry* **2001**, *40*, 3037−3046.

(24) Allin, C.; Ahmadian, M. R.; Wittinghofer, A.; Gerwert, K. *Proc. Natl. Acad. Sci.* **2001**, *98*, 7754−7759.

(25) Baril, J.; Max, J.-J.; Chapados, C. *Can. J. Chem.* **2000**, *78*, 490−507.

(26) Becke, A. D. *Phys. Rev. A* **1988**, *38*, 3098−3100.

(27) Perdew, J. P. *Phys. Rev. B* **1986**, *33*, 8822−8824.

(28) Boesch, S. E.; Wheeler, R. A. *J. Phys. Chem.* **1995**, *99*, 8125−8134.

(29) Hertwig, R. H.; Koch, W. *J. Comput. Chem.* **1995**, *16*, 576−585.

(30) Becke, A. D. *J. Chem. Phys.* **1993**, *98*, 1372−1377, 5648−5652.

(31) Lee, C.; Yang, W.; Parr, R. C. *Phys. Rev. B* **1988**, *37*, 785−789.

(32) Hartwigsen, C.; Goedecker, S.; Hutter, J. *Phys. Rev. B* **1998**, *58*, 3641−3662.

(33) Jorgensen, W. L.; et al. *J. Chem. Phys.* **1983**, *79*, 926−935.

(34) Brooks, B. R.; Bruccoleri, R. E.; Olafson, B. D.; States, D. J.; Swaminathan, S.; Karplus, M. *J. Comput. Chem.* **1983**, *4*, 187−217.

(35) Neria, E.; Fischer, S.; Karplus, M. *J. Chem. Phys.* **1996**, *105*, 1902−1921.

(36) Berendsen, H. J. C.; Postma, J. P. M.; van Gunsteren, W. F.; DiNola, A.; Haak, J. R. *J. Chem. Phys.* **1984**, *81*, 3684−3690.

(37) Mathias, G.; Egwolf, B.; Nonella, M.; Tavan, P. *J. Chem. Phys.* **2003**, *118*, 10847−10860.

(38) Niedermeier, C.; Tavan, P. *J. Chem. Phys.* **1994**, *101*, 734−748.

(39) Niedermeier, C.; Tavan, P. *Mol. Simul.* **1996**, *17*, 57−66.

(40) Herres, W.; Gronholz, J. *Comput. Appl. Lab.* **1984**, *2*, 216−220.

(41) Laasonen, K.; Sprik, M.; Parrinello, M.; Car, R. *J. Chem. Phys.* **1993**, *99*, 9080−9089.